An Assessment of the Differential Inversion Method for Remote Sounding of Temperatures

S. C. OU AND K. N. LIOU

Department of Meteorology/CARSS, University of Utah, Salt Lake City, Utah

J. F. KING

Division of Atmospheric Studies, Geophysics Directorate, Phillips Laboratory, Hanscom Air Force Base, Massachusetts

(Manuscript received 1 July 1992, in final form 7 December 1992)

ABSTRACT

We have explored the applicability of the differential inversion (DI) method to temperature retrievals in both clear and cloudy atmospheres using real satellite data. The main theme of the DI is that the local Planck intensity can be exactly expressed by a linear combination of the derivatives of radiances in the logarithmic pressure coordinate. The inversion coefficients are obtained by fitting the weighting function to a generalized form. The higher-order derivatives of radiances are determined from polynomial fittings. The satellite dataset used in this work contains collocated brightness temperatures and radiosonde data that have been collected during the period of Baseline Upper Atmospheric Network (BUAN) experiments. These data include both cloudy and clear cases. A multispectral cloud-removal method using the principle of the N^* method has been developed. This method uses radiances of High-Resolution Infrared Radiation Sounder channels 6, 7, and 8 to estimate clear radiances of these channels and the surface temperature simultaneously based on radiative transfer simulations. Subsequently, the quantity N^* (the ratio of effective cloud cover over adjacent pixels) and the clear radiances of the rest of the channels are evaluated.

Retrieval results are presented in terms of rms temperature differences between retrieved and sounding profiles. Considering all clear and partly cloudy cases, the rms differences in temperature of approximately 2 K for retrievals using the DI are comparable to those using the minimum-variance scheme. The rms differences in temperature for retrievals using the multispectral cloud-removal scheme are slightly larger than those using the BUAN cloud-removal scheme by approximately 0.5 K. Finally, the rms temperature differences are much smaller than those for the first guess of the minimum-variance scheme. These results indicate first that the DI can achieve acceptable performance without first-guess or error covariance matrices; second, that the proposed multispectral cloud-removal method is also capable of generating reasonable cloud-removed clear radiances; and finally that the DI can be used as a tool to obtain first guesses in the current operational method and to perform large-volume temperature retrievals for climate studies.

1. Introduction

Although operational retrievals of temperature profiles have been routinely performed in the past 15 years, the techniques and procedures used have been under constant refinement. The need for refinement arises from the complicated nature of the problem, in which consistent and accurate performance is difficult to achieve. The many retrieval methods proposed in the past can be categorized into two groups: statistical and physical methods.

Statistical methods determine temperature profiles based on results from regression analyses of collocated satellite and sounding data. While statistical methods are computationally fast, the accuracy of the retrieved temperatures varies significantly. Physical methods determine temperature profiles by solving an ill-conditioned and ill-posed Fredholm integral equation of the first kind. Because of the unstable characteristics of the solution process, conventional physical methods prescribe first-guess profiles and specify external constraints to control the behavior of the solution. For example, the minimum-variance (MV) scheme (Fleming et al. 1986; Eyre 1989) utilizes numerical weather prediction models or statistical library search procedures to generate first guesses and uses the elements of error covariance matrices to control the smoothness of the resulting temperature profiles. Other physical methods involve nonlinear iterations, which assume certain relationships between radiances and Planck intensities (Smith 1970; Chahine 1970).

Many attempts have been made to improve and refine the performance of various aspects of the atmospheric temperature retrievals. For example, in the

Corresponding author address: Dr. Szu-Cheng S. Ou, CARSS/Department of Meteorology, University of Utah, 809 William C. Browning Bldg., Salt Lake City, UT 84112.

Baseline Upper Atmospheric Network (BUAN) experiment, it was theorized that better collocation of satellite and sounding data would lead to better retrievals. For this reason, the size of temporal and spatial collocation windows were reduced from ±3 h and ±300 km to ±1 h and ±150 km. However, no significant retrieval improvements were achieved (Bloom and Nappi 1990). It has also been suggested that increasing the number of sensing channels may yield additional information content for temperature retrievals and improve retrieval accuracy. Along this line, simulation studies based on the Advanced Moisture and Temperature Sounders (AMTS) showed that better retrievals can be achieved by using high-resolution channels (Phillips et al. 1988). Smith et al. (1990) demonstrated that rms temperature errors can be reduced to 1–1.5 K by using hundreds of channels on the High-Resolution Interferometer Sounder (HIS) on board aircraft. However, only limited cases for a short time interval and over a small geographical locality have been tested. There are also a number of studies focusing on searching for improved first-guess profiles (e.g., McMillin 1991; Chedin et al. 1985).

In an attempt to circumvent the requirement for first guess, King (1985) proposed a novel linear transform approach to solve the temperature retrieval problem. This approach is referred to as the differential inversion method (DI). The essence of the DI is that, based on the convolution theory, the Laplace transform of the Planck intensity profile is linearly related to the Laplace transform of radiance profile. By applying the inverse transform, the local Planck intensity can be expressed as a linear combination of the derivatives of radiances in the logarithmic peak pressure coordinate. Instead of using external constraints to "regularize" the retrieved temperature profile, it is assumed that the radiances can be represented by smooth polynomial functions, so that the derivatives of radiances can be computed. Thus, the DI offers an alternative approach for solving the temperature retrieval problem, in that the prescription of the first-guess profile and the associated error covariance matrices are not required.

It has been shown that the DI is efficient, stable, and particularly practical for narrow weighting functions (Ou and Liou 1989; King et al. 1989). The purpose of this work is to further examine the applicability of the DI to temperature retrievals. Section 2 presents the fundamentals of the DI. The BUAN dataset is used to test whether the DI can be applied to the retrieval of atmospheric temperature profiles using satellite data. Details of the BUAN dataset are given in section 3. To apply the DI to temperature retrievals in partly cloudy atmospheres, clear radiances must be reconstructed from cloud-contaminated radiances. Many cloud-removal methods have been proposed in conjunction with various retrieval schemes. Most of these methods follow the principles of the N^* method (Smith 1968). We have developed a new approach that uses High-Resolution Infrared Radiation Sounder (HIRS) channels 6, 7, and 8 radiances to determine surface temperature, clear radiances, and N^* simultaneously based on results from radiative transfer simulations. Details of the cloud-removal method are discussed in section 4. While the DI is a linear inversion method, the problem involving atmospheric temperature retrievals using satellite data is highly nonlinear. To apply the DI to temperature retrievals using either clear or cloud-removed radiances, these radiances must be adjusted so that major nonlinear components are removed. The adjustment of radiances appears in section 5. Retrieval results and discussions are provided in section 6, and conclusions are presented in the final section.

2. Fundamentals of the differential inversion method

a. Forward radiative transfer equation

The upwelling radiance at the top of the atmosphere, R_ν, for a given spectral band may be derived from the solution of the basic radiative transfer equation. Assuming a plane-parallel atmosphere under local thermodynamic equilibrium, we have

$$R_\nu = B_\nu(T_s)T_\nu(p_s) + \int_{p_s}^{0} B_\nu(p)\frac{\partial T_\nu(p)}{\partial p}\,dp, \quad (1)$$

where B_ν is the Planck intensity at central wavenumber ν, T_ν is the transmittance, p_s is the surface pressure, and T_s is the surface temperature. The first and second terms represent surface and atmospheric emission contributions, respectively.

The slab below the surface may be viewed as a semi-infinite isothermal emitter whose temperature is T_s, and whose pressure increases from p_s downward to ∞. For $p \to \infty$, $T_\nu(\infty)$ is taken to be 0. Thus $T_\nu(p_s)$ can be expressed by the following mathematical identity:

$$T_\nu(p_s) = T_\nu(p_s) - T_\nu(\infty) = \int_{\infty}^{p_s}\frac{\partial T_\nu(p)}{\partial p}\,dp. \quad (2)$$

Multiplying both sides of Eq. (2) by $B_\nu(T_s)$, we obtain

$$B_\nu(T_s)T_\nu(p_s) = \int_{\infty}^{p_s} B_\nu(p_s)\frac{\partial T_\nu(p)}{\partial p}\,dp. \quad (3)$$

Combining Eqs. (1) and (3) leads to the following forward radiative transfer equation in continuous form:

$$R_\nu = \int_{\infty}^{0} B_\nu(p)\frac{\partial T_\nu(p)}{\partial p}\,dp, \quad (4)$$

where $B_\nu(p) = B_\nu(T_s)$ for $p_s < p < \infty$.

We next define the weighting function as the negative logarithmic derivative of the transmittance:

$$W_\nu(p) = -p\frac{\partial T_\nu(p)}{\partial p}. \quad (5)$$

The weighting function controls the relative contribution of atmospheric emission from various levels and

depends on the vertical distribution of absorbing gases and temperature.

b. Differential inversion method

We shall approach the inverse problem by a transformation of variables. The following variables are introduced: $\bar{\xi} = -\ln\bar{p}$ and $\xi = -\ln p$, where $\bar{p}$ is the peak pressure of the weighting function W. In terms of these new variables, Eq. (4) can be rewritten as (King 1985; Ou and Liou 1989)

$$R(\bar{\xi}) = \int_{-\infty}^{\infty} B(\xi)W(\xi - \bar{\xi})d\xi, \tag{6}$$

where $R(\bar{\xi}) = R_\nu(\bar{p})$, $B(\xi) = B_\nu(p)$, and $W(\xi - \bar{\xi}) = W(p, \bar{p})$. Assume that R is some smooth function of the variable $\bar{\xi}$, for which higher-order derivatives exist. This assumption implies that for each value of $\bar{\xi}$, there is a corresponding weighting function $W(\xi - \bar{\xi})$. Subsequently, we perform a bilateral Laplace transform (Widder 1971) on both sides of Eq. (6), and use the convolution theory to obtain

$$r(s) = b(s)w(-s), \tag{7}$$

where s denotes the transform variable, and $r(s)$, $b(s)$, and $w(-s)$ represent the bilateral Laplace transforms of R, B, and W, respectively. Based on Eq. (7), we can obtain $B(\bar{\xi})$ as follows:

$$B(\bar{\xi}) = L^{-1}\left[\frac{r(s)}{w(-s)}\right], \tag{8}$$

where L^{-1} is the inverse bilateral Laplace transform. The term $1/w(-s)$ may be expanded into a MacLaurin series (Pearson 1974) so that

$$\frac{1}{w(-s)} = \sum_{n=0}^{\infty} \lambda_n s^n, \tag{9}$$

where the coefficient λ_n is related to the nth derivative of the function $1/w(-s)$ evaluated at $s = 0$ as follows:

$$\lambda_n = \frac{1}{n!}\left[\frac{1}{w(-s)}\right]^{(n)}_{s=0}. \tag{10}$$

By inserting Eq. (9) into Eq. (8), and noting that λ_n's are constants, we have

$$B(\bar{\xi}) = \sum_{n=0}^{\infty} \lambda_n L^{-1}[s^n r(s)]. \tag{11}$$

We may use expressions for the Laplace transform of the nth derivative of the function $R(\bar{\xi})$ to determine the inverse transform of $s^n r(s)$. Using this procedure, $B(\bar{\xi})$ can be expressed in terms of a linear sum of radiance derivatives at $\bar{\xi}$ as follows:

$$B(\bar{\xi}) = \sum_{n=0}^{\infty} \lambda_n \frac{d^n R(\bar{\xi})}{d\bar{\xi}^n}. \tag{12}$$

In order to evaluate higher derivatives on the right side of Eq. (12), $R(\bar{\xi})$ must be a smooth function of $\bar{\xi}$. In principle, the solution of $B(\bar{\xi})$ becomes mathematically exact for infinite summations. However, for narrow weighting functions, λ_n converges rapidly to zero, so that the summation of Eq. (12) may be truncated to just a few terms.

c. Weighting functions and inversion coefficients

The determination of $B(\bar{\xi})$ from Eq. (12) requires knowledge of both λ_n and the derivatives of $R(\bar{\xi})$. The inversion coefficient λ_n depends on the weighting function W. The bilateral Laplace transform of W can be expressed by

$$w(-s) = \int_0^{\infty} \tilde{p}^{-s} W(\tilde{p}) \frac{d\tilde{p}}{\tilde{p}}, \tag{13}$$

where $\tilde{p} = p/\bar{p}$. In principle, if the atmospheric temperature and humidity profiles are known, it is then possible to evaluate w, and subsequently $1/w(-s)$ and its derivatives numerically through accurate line-by-line spectral integrations. However, because atmospheric parameters are not known before retrieval, the above numerical approach is not practical, and we prefer to develop an analytic form that can adequately approximate the weighting functions. A generalized weighting function has been proposed by King (1985) in the form

$$W_\kappa(\tilde{p}) = \kappa^{(\kappa-1)/\kappa}\Gamma^{-1}\left(\frac{1}{\kappa}\right)\tilde{p}\exp\left(-\frac{\tilde{p}^\kappa}{\kappa}\right), \tag{14}$$

where Γ is the gamma function and κ, which is an index controlling the sharpness of the weighting function, is independent of the temperature profile. Figure 1 shows the functional form of W_κ for $\kappa = 0.5$, 1, and 2. Smaller values of κ correspond to broader weighting functions with lower peak values. The range of significant contribution of the weighting function is from $\tilde{p} = 0.1$ to $\tilde{p} = 10$, spanning two orders of magnitude.

Using the functional form of Eq. (14), we can show that

$$w(-s) = \frac{\Gamma[(1 - s)/\kappa]}{\Gamma(1/\kappa)\kappa^{s/\kappa}}. \tag{15}$$

Evaluation of $w(-s)$, and therefore of λ_n, based on Eqs. (13) and (10) involves digamma and polygamma functions (Abramowitz and Stegun 1972). Expressions for λ_n as functions of κ have been given by King (1985) for $n = 1$–5. Figure 2 shows the inversion coefficients λ_n for $n = 1$–5 as functions of κ. For $\kappa > 1$, $-1 < \lambda_n < 0.2$, and λ_n decreases in magnitude as κ increases. In addition, based on Eq. (12), any error inherent in the derivatives of $R(\bar{\xi})$ would be substantially suppressed in the retrieved $B(\bar{\xi})$, because λ's converge to zero for larger n. For $\kappa < 1$, $|\lambda_1|$, $|\lambda_3|$, and $|\lambda_5|$ are still less than 1, but $|\lambda_2|$ and $|\lambda_4|$ increase sharply with de-

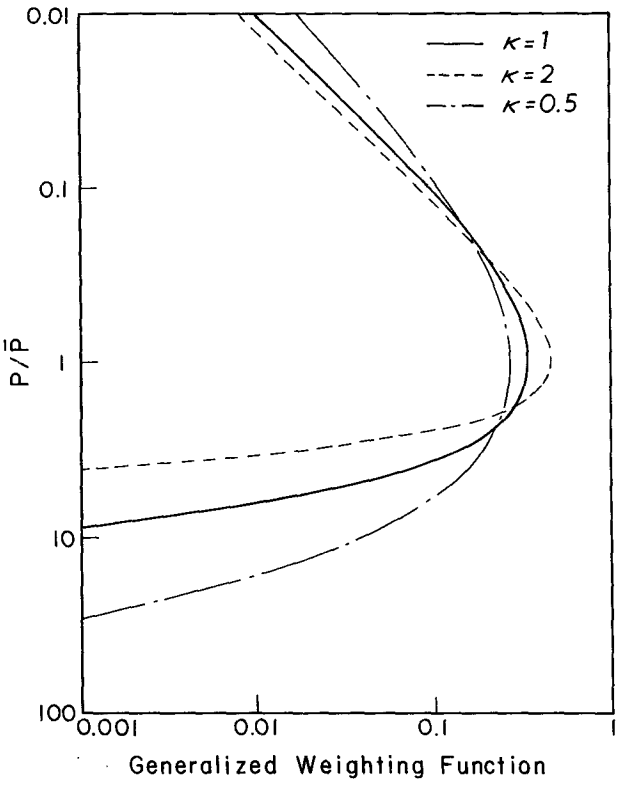

FIG. 1. The generalized weighting function as a function of $p/\bar{p}$ for the sharpness index $\kappa = 0.5$, 1, and 2.

creasing κ. Errors in radiances will then be amplified through λ_2 and λ_4 and propagate into the computation of $B(\bar{\xi})$.

d. Polynomial representation of radiance profiles

Evaluation of higher derivatives of $R(\bar{\xi})$ is based on the condition that radiances can be represented by smooth functions in terms of the variable $\bar{\xi}$. In principle, a large variety of smooth functions can be used for representing the radiance profile. The optimal functional form should be based on physical reasoning and should give an exact solution for the Planck intensity profile (Houghton et al. 1984). Chandrasekhar (1960) showed that the upwelling radiance from an infinite atmosphere is a linear combination of hyperbolic functions. King and Leon (1990) developed an algorithm to apply this hyperbolic form to temperature retrieval. However, Chandrasekhar's original theory applies to an infinite atmosphere. Although the radiative transfer equation can be modified to simulate infinite atmospheres [Eq. (4)], the exponential Planck profile derived by King and Leon cannot properly account for the discontinuity at surface and the isothermal behavior for $p > p_s$. Since the solution of the radiative transfer equation can be expressed in a series of exponential functions in terms of the optical depth, and since the exponential function can be expanded in polynomials, the upwelling radiance may be written in terms of polynomials. An ordinary form of polynomial is used. Other types of polynomials that are the solutions of differential equations (e.g., Chebyshev, Legendre, etc.) can be converted into an ordinary form. Spline polynomials are not used because exact fittings of radiance subsets would be involved. These fittings may lead to numerical instability in the solution of the ill-conditioned integral equation.

We may express $R(\bar{\xi})$ using an Nth-degree polynomial of $\bar{\xi}$ in the form

$$R(\bar{\xi}) = \sum_{m=0}^{N} a_m \bar{\xi}^m. \tag{16}$$

Substituting Eq. (16) into Eq. (12) leads to

$$B(\bar{\xi}) = \sum_{n=0}^{N} \lambda_n \sum_{m=n}^{N} \frac{m! a_m}{(m-n)!} \bar{\xi}^{m-n}. \tag{17}$$

Equation (17) is also an Nth-degree polynomial. Equations (16) and (17) contain excellent algebraic reciprocal properties for the inverse and forward problems. As will be shown later, the polynomial form of $B(\bar{\xi})$ fits the atmospheric Planck intensity profile well, and for $p > p_s$, its moderate deviation from isothermal behavior can be accounted for by the adjustment of radiances.

To compute $B(\bar{\xi})$, we only need to know the $N+1$ coefficients a_m in Eq. (16). In practice, only a finite

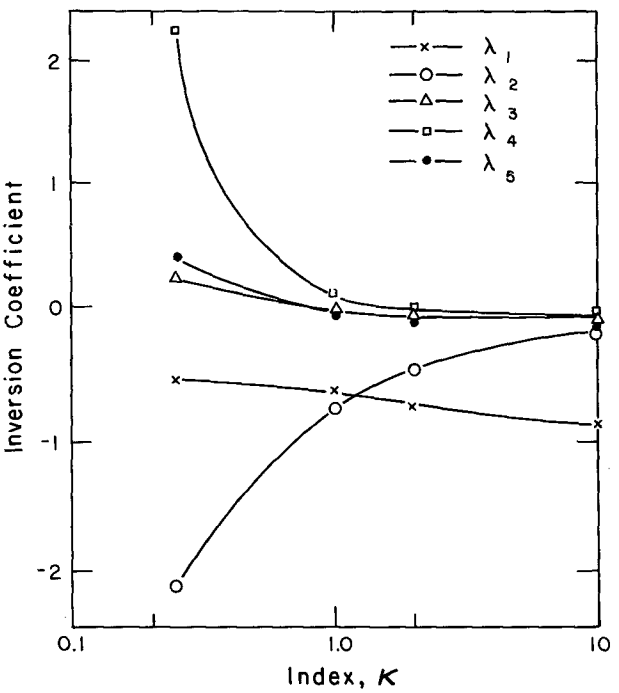

FIG. 2. Inversion coefficients λ_i ($i = 1$–5) as functions of the index κ.

number of measured radiances are available. The unknown polynomial coefficients in Eq. (16) must be obtained by numerical fitting of the finite number of $R(\bar{\xi}_i)$. These coefficients are mathematically accurate and unique with respect to a specific set of radiances. Errors are inherent in the clear radiances derived from measurements. Possible error sources include instrument noises and viewing angle correction. Both the measured radiances and the inherent errors are fitted to a single polynomial. However, the effects of errors on the retrieved profiles are small for the following reasons. First, the instrument noises in radiances for HIRS channels 1–7 and 13–17 are all less than 1% and errors due to viewing angle correction can be reduced by using detailed radiative transfer models. Second, the DI is numerically stable with respect to errors in radiances that do not propagate into the retrieved solution.

3. Dataset used in temperature retrieval studies

We have acquired from the National Environmental Satellite, Data, and Information Service (NESDIS) a large dataset of collocated temperature profiles and satellite data. These data were collected during the observation period (15 January–15 July 1988) of the BUAN experiment. We were also provided with the transmittance model currently being used in NESDIS which computes atmospheric transmittances due to the absorption by water vapor continuum and rotational bands, CO_2 15-μm band, and ozone 9.6-μm band for the 19 HIRS channels (McMillin et al. 1979). A brief description of the BUAN dataset is given below.

a. Satellite data

The BUAN dataset contains satellite data measured by the infrared and microwave radiometers on board *NOAA-10*. The data of *NOAA-9* were not available during the field experiment due to an instrument malfunction. There are two levels of the dataset. The level 1-T (match file B) contains original brightness-temperature data for the 19 HIRS, 4 Microwave Sounding Unit (MSU), and 3 Stratospheric Sounding Unit (SSU) channels. These brightness-temperature data have been converted from counts recorded by the radiometer for all weather conditions, including clear, partly cloudy, and overcast situations. Each record contains the sounder data over a "box" which consists of an array of 11 × 9 spots. An example of the display of the array is shown in Fig. 3. Only the data for the 9 × 7 spots within the solid frame of Fig. 3 are subject to retrieval analysis. These 9 × 7 spots are further divided into six miniboxes. At most, one retrieval is done for each minibox. The point of retrieval is determined through a series of tests. One or more radiosonde stations are also located within the domain of the 9 × 7 spots ("+" in the diagram). The distance between retrieval point and the radiosonde station is less than 150 km. In Fig. 3, five of the six miniboxes produce retrieval points. Only one minibox produces no retrieval point, because all points in that minibox are more than 150 km away from the radiosonde station. The BUAN retrieval procedures using the MV have been documented by Reale et al. (1990).

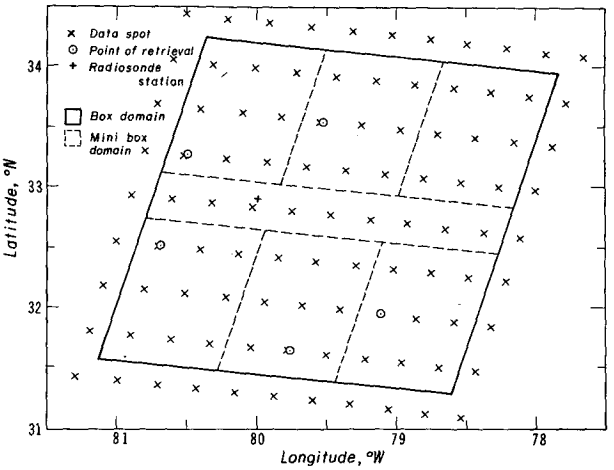

FIG. 3. Display of the array of 11 × 9 spots in a box. Each "×" denotes one spot. Cloud-clear analyses are performed for the 9 × 7 spots within the solid frame. These spots are further divided into six miniboxes. Only one retrieval is done for each minibox. The spot over which a retrieval is performed is denoted by "O." The rawinsonde station is denoted by "+." The distance between the station and the retrieval spot is less than 150 km.

The other level of data (match file A) contains the BUAN retrieval products. These include specifications of the spot for which retrievals are performed, the associated latitude, longitude, date, time, the original or cloud-removed clear radiances, the retrieved temperature and humidity profiles, the average value of N^* (used in the cloud-removal scheme), surface albedo, skin temperature, surface elevation, and first-guess temperature and humidity profiles. It is noted that the original clear radiances are directly adopted from the brightness temperatures for an identified clear spot, and that the "cloud-removed" clear radiances are generated from the BUAN N^* method.

b. Collocated dataset of radiosonde observations

BUAN radiosonde and satellite observations were collocated and saved each day during the period of data collection. The general procedure was to collect pairs of radiosonde and satellite observations that were within 1 h and 150 km of each other. [The normal operational collocation window is ±3 h and ±300 km (Kalnay et al. 1990).] The radiosonde data contains vertical profiles of pressure, temperature, dewpoint depression, geopotential height, wind direction, and wind speed. These data were recorded in terms of 15 mandatory (all data) and 25 significant (temperature and pressure only) levels.

4. Cloud-removal method

We have developed a method to restore clear radiances from cloud-contaminated brightness temperatures based on the principle of the N^* method, where the quantity N^* is the ratio of effective cloud covers over a pair of adjacent pixels. The current method differs from other N^* methods in that N^* is determined using the radiances involving HIRS channels 6, 7, and 8 based on radiative transfer simulations. A detailed description of the current cloud-removal method is given below.

a. N method*

For a pair of adjacent pixels, let the radiances for the ith channel over clear and cloudy areas be R_{0i} and R_{ci}, respectively. Then the radiances for pixels 1 and 2 are given by

$$R_{i1} = (1 - \eta_1)R_{0i1} + \eta_1 R_{ci1}, \quad (18a)$$

$$R_{i2} = (1 - \eta_2)R_{0i2} + \eta_2 R_{ci2}, \quad (18b)$$

where η_1 and η_2 are the effective cloud covers for the respective pixels. These effective covers are defined as the product of cloud cover and emissivity. We have assumed that over each of the adjacent pixels only a single layer of cloud is present and that clouds are located at the same altitude with the same cloud temperature. In addition, clouds are assumed to have the same radiative properties. This assumption is generally valid for water clouds that are thermally black. The surface and clear atmospheric conditions over the adjacent pixels are also assumed to be the same. The above assumptions lead to the approximations $R_{0i1} = R_{0i2} = R_{0i}$ and $R_{ci1} = R_{ci2} = R_{ci}$. Consequently, we can eliminate R_{ci} from Eqs. (18a) and (18b) and obtain

$$N^* = \frac{\eta_1}{\eta_2} = \frac{R_{0i} - R_{i1}}{R_{0i} - R_{i2}}. \quad (19)$$

If we know N^* in advance, we may determine R_{0i} from Eq. (19) as follows:

$$R_{0i} = \frac{R_{i1} - R_{i2}N^*}{1 - N^*}. \quad (20)$$

The N^* method is subject to the following restrictions: 1) the assumption that adjacent clouds are of the same height, temperature, and radiative properties; 2) the N^* method cannot be used when both pixels have the same amount of cloud cover—in this case, $N^* = 1$ and the denominator in Eq. (20) becomes infinite; 3) the N^* method will also fail when an inversion is present in the temperature profile, in this case, $R_{i1} \sim R_{i2} \sim R_{0i}$; 4) additional information is required to determine R_{0i}. This information can be extracted from the radiance of a channel that is not used in the temperature retrieval. The conventional approach is to use microwave channel radiance. However, microwave measurements are usually subject to errors caused by poor resolution, contamination by precipitating clouds, and uncertainties in the estimated surface emissivity.

b. Multispectral cloud-removal scheme

We have developed a multispectral approach using the HIRS channel 6, 7, and 8 radiances to determine the surface temperature and clear radiances simultaneously. Channel 8 is the window channel and is not used in temperature retrieval. First, radiative transfer simulations are performed to establish parameterization relationships between clear radiances of the three channels. The relationships between partly cloudy radiances of the same channels are next examined. Finally a set of algebraic equations are subsequently derived and solved based on simulation analyses.

1) MULTISPECTRAL CORRELATION OF CLEAR RADIANCES

To economize the computational effort involving the calculation of clear radiances, parameterization relationships of clear radiances have been developed for channels whose weighting functions peak near the surface. The BUAN temperature and humidity sounding profiles have been used to perform simulation studies. The parameterizations are developed using $\Delta R_i = R_{si} - R_{0i}$, where R_{0i} and R_{si} are the clear radiance and surface-emitted radiance for channel i.

Figures 4a and 4b show the relationships of ΔR_7 versus ΔR_6 and ΔR_8 versus ΔR_7, respectively. The quantities R_{0i} are obtained based on radiative transfer simulations using a large number of temperature and humidity profiles contained in the BUAN dataset. Weighting functions are computed using the NESDIS transmittance model. The correlation between the channels 6 and 7 radiance difference is extremely good, and its dependence on surface temperature and humidity appears to be minimal for $\Delta R_6 < 40$ mW m^{-2} sr^{-1} cm^{-1}. For $\Delta R_6 > 40$ mW m^{-2} sr^{-1} cm^{-1}, the computed points exhibit a larger spread, which is within only 3 mW m^{-2} sr^{-1} cm^{-1}. We theorize that the spread is due to increasing humidity variations in the warmer air. The solid curve in Fig. 4a is the quadrature fit in the form

$$\Delta R_7 = \sum_{n=0}^{2} d_n \Delta R_6^n, \quad (21)$$

where $d_0 = 0.5763$, $d_1 = 0.3736$, $d_2 = 0.0047$. The rms difference between the simulated and fitted values of ΔR_7 is about 1 mW m^{-2} sr^{-1} cm^{-1}. Thus Eq. (21) is a reasonable representation of the correlation between the channels 6 and 7 radiance differences. On the other hand, the correlation between the channels 7 and 8 radiance differences, as shown in Fig. 4b in log–log

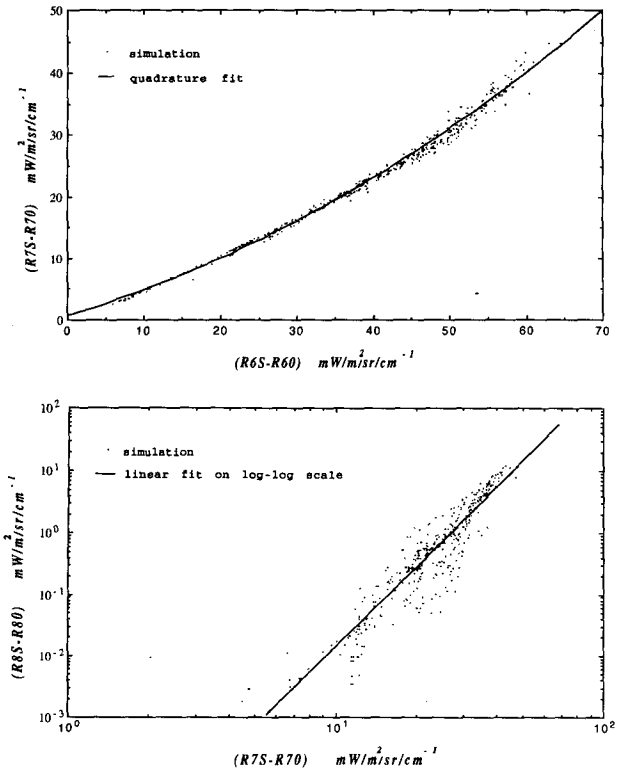

FIG. 4. Correlations between (a) ΔR_7 and ΔR_6 and (b) ΔR_8 and ΔR_7.

plot, is less satisfactory. A parameterization equation relating ΔR_8 and ΔR_7 has been derived as follows:

$$\ln\Delta R_8 = e_0 + e_1 \ln\Delta R_7, \qquad (22)$$

where $e_0 = -14.33$ and $e_1 = 4.35$. The rms difference between the simulated and fitted values of ΔR_8 is about 1 mW m^{-2} sr^{-1} cm^{-1}.

2) Relationship between partly cloudy radiances of selected channels

The N^* method is based on the assumption that the partly cloudy radiance for a particular pixel is a linear function of the cloud cover η. Given that N^* is constant for all channels, we may derive from Eq. (19) the following equation:

$$\frac{R_{0i} - R_{i1}}{R_{0j} - R_{j1}} = \frac{R_{0i} - R_{i1}}{R_{0j} - R_{j2}} = G_{ij}. \qquad (23)$$

Further mathematical manipulations of Eq. (23) lead to

$$G_{ij} = \frac{R_{i1} - R_{i2}}{R_{j1} - R_{j2}}. \qquad (24)$$

The unknown R_{0i} and R_{0j} are eliminated, so that G_{ij} can be estimated from known values of R_{i1}, R_{i2}, R_{j1}, and R_{j2}. Once G_{ij} is obtained, a linear relationship between R_{0i} and R_{0j} can be established based on Eq. (23). This linear relationship can be used in conjunction with Eqs. (21) and (22) to solve for clear radiances. However, Eqs. (23) and (24) are valid only when the assumptions made in the N^* method are valid, that is, the cloud properties are the same over adjacent pixels. Thus to apply the multispectral method to a sample of adjacent pairs (e.g., the 3 × 3 arrays in Fig. 3), we must select the most appropriate value of G_{ij}. This is described in the next subsection.

3) Estimate of G_{ij}

Figure 5 illustrates the principles of the optimal estimation of G_{ij}. Shown in the diagram is a two-dimensional display of channels 6 and 7 radiances. The inset in the upper-left portion of the diagram is a 3 × 3 array of numbered pixels. The 3 × 3 array represents one basic working unit of the cloud-removal scheme. As shown in Fig. 3, for a given point of retrieval a 3 × 3 array can be constructed where the point of retrieval is the center pixel. Eight pairs of adjacent pixels are formed by pairing the center pixel (number 9) with eight surrounding pixels. The nine radiance points corresponding to the pixels are plotted along with the Planck intensity curve. Their values are smaller than the corresponding clear radiances (R_{07}, R_{06}) because the cloud temperature is usually lower than below-cloud atmospheric temperature. The scatter of the points signifies a typical situation of different cloud properties for different pixels. Let the point for clear radiances be denoted as "0," which should also fall on the clear radiance curve [Eq. (21)]. The point (R_{s6}, R_{s7}) is the intersect between the clear radiance curve and the Planck intensity curve and corresponds to the surface emission.

To obtain the optimal estimate of G_{ij}, we construct a straight line that passes through the pair of points with the largest distance. Its slope is our best estimate

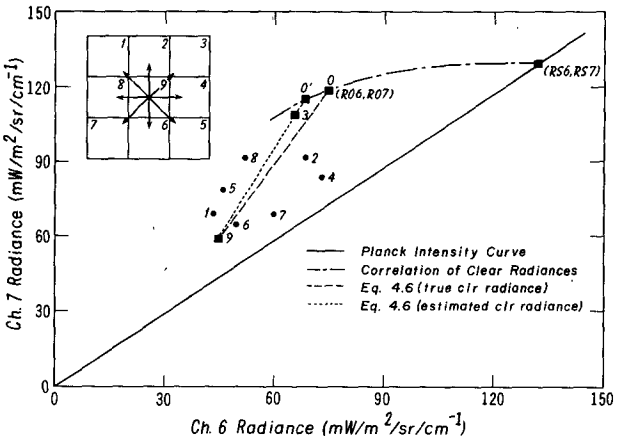

FIG. 5. Conceptual diagram illustrating the strategy for selecting the optimal pair of pixels and the associated G_{ij}.

of G_{ij}, and its intersect with the clear radiance curve is our solution for the clear radiances. In Fig. 5, points 3 and 9 show the largest distance. The slope of $\overline{93}$ (the straight line connecting 9 and 3) is close to that of $\overline{90}$. Using the slope of $\overline{93}$ as G_{76}, we obtain a solution for the clear radiance at 0′. Evidently, 0′ is close to 0. Straight lines that connect point 9 with other points will intersect the clear radiance curve farther away from 0. The example shown here is an ideal case. This strategy does not guarantee the accuracy of the derived clear radiances. In particular, if all the radiance points are close to each other, the estimated G_{ij} may still have a large error. Thus, additional restrictions are required to filter out unreasonable values of G_{ij}.

The range of G_{ij} may be obtained from simulation studies using the NESDIS transmittance program. The cloud cover and cloud-top pressure are prescribed randomly for each atmospheric profile, and the clear radiances are computed. The cloudy radiances are computed based on the following equation:

$$R_{ci} = B_\nu(T_c)T_\nu(p_c) + \int_{p_c}^{0} B_\nu(p)\frac{\partial T_\nu(p)}{\partial p}\,dp, \qquad i = 6, 7, 8, \quad (25)$$

where p_c and T_c are cloud-top pressure and temperature, respectively. Partly cloudy radiances are obtained from Eq. (18a). Finally, G_{76} is obtained from Eq. (23) using the simulated clear and partly cloudy radiances. We found that the simulated values of G_{76} and G_{87} are between 1.0 and 3.0. Also, G_{ij} increases with p_c. In fact, it can be shown that G_{ij} is the cloud pressure function used in the CO_2 slicing method to determine cloud pressure (McCleese and Wilson 1976; Smith and Platt 1978; Wielicki and Coakley 1981; Menzel et al. 1983). The cloud pressure function is defined as the ratio of radiance differences between clear and cloudy conditions for two different IR channels. In general, the computed values of G_{ij} are always larger than 1.0. The maximum value of G_{ij} depends on the wavelength of the two channels. Based on the above analysis, any G_{ij} determined from Eq. (24) with a value larger than 3.0 or less than 1.0 is rejected.

Once the G_{ij} is determined, we simultaneously solve Eqs. (21), (22), and (23) for clear radiances of channels 6, 7, and 8 and surface temperature. An efficient numerical iterative scheme has been developed for this purpose.

5. Application of DI to temperature retrieval

a. HIRS channel characteristics

In order to investigate the potential applicability of DI, HIRS channels (Smith et al. 1979) are used to perform the temperature retrieval. HIRS consists of 19 channels: channels 1–7 are in the CO_2 15-μm band, channel 8 is in the 11-μm-window band, channel 9 is in the O_3 9.6-μm band, channels 10–12 are in the water vapor vibration–rotation band, channels 13–17 are in the CO_2 4.3-μm band, and finally, channels 18 and 19 are in the 3.7-μm-window band. For the purpose of temperature retrieval, the seven channels in the CO_2 15-μm band and the five channels in the CO_2 4.3-μm band will be used. It is noted that the weighting functions of channels 1–3 and 17 peak in the stratosphere ($\bar{p} \leq 100$ mb).

b. Parameters of weighting functions

The generalized weighting function defined in Eq. (14) is used in the retrieval analysis. The key parameters in this function are κ and $\bar{p}$. The BUAN temperature and humidity profiles and the NESDIS transmittance model are used to compute a large number of weighting function profiles for HIRS channels 1–7 and 13–17. We then use a least-square method to fit each weighting function to the generalized form to determine κ and $\bar{p}$. Based on the transmittance calculations, most of the weighting functions for the HIRS temperature channels are smooth and singly peaked for average atmospheric conditions. The prime contribution to the radiance comes from emission near the weighting function peak. Thus, it is not necessary to fit the entire weighting function profile, but to obtain accurate fitting near the peak. From all κ and $\bar{p}$ values, we obtain mean values and the associated standard deviations for each channel, which are shown in Fig. 6. It is evident that the κ values for channels 1–5 and 14–17 are smaller than 2 with standard deviations less than 0.5, indicating broader but less-variant weighting functions. In contrast, these values for channels 6, 7, and 13 are all greater than 2 with standard deviations larger than 1.5. Variations in κ for channels 6, 7, and 13 are primarily associated with water vapor absorption and emission in the lower troposphere. The range of $\bar{p}$ is generally within 70 mb. From numerical experi-

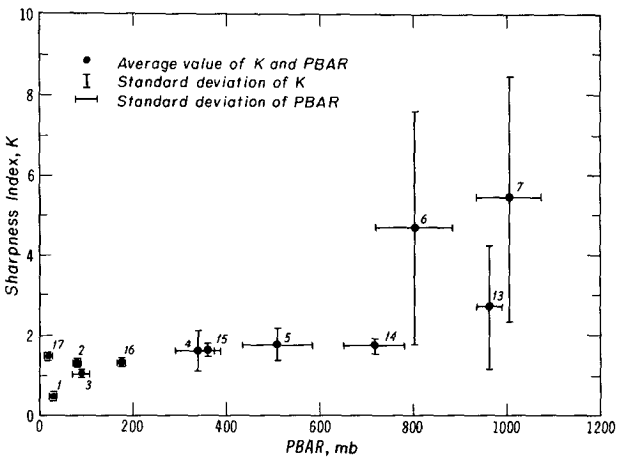

FIG. 6. Distribution of the mean sharpness index κ and the peak pressure $\bar{p}$. The vertical and horizontal bars denote standard deviation for κ and $\bar{p}$, respectively. The numerals denote the channel number.

ments, the κ and $\bar{p}$ are largely independent of the temperature and humidity profiles. The computations of these two parameters are performed off-line of the retrieval program. Their mean values are used to establish a universal equation for adjusting the observed radiances to filter out all of the possible nonlinear factors.

c. *Optimal degree of polynomial fitting of radiances*

The selection of the degree of polynomial fitting is a critical factor for the success of DI in temperature retrieval. Figure 7 illustrates the principles of the search for the optimal degree of polynomial fitting, using the simulated radiances of the seven 15-μm HIRS channels that are generated based on the U.S. standard atmospheric profile. They are fitted to polynomials of different degrees (third, fifth, and sixth). The accuracy of the fitting improves as the degree of the polynomial increases. The sixth-degree fitting is the exact fit for the seven radiances. An important assumption in DI, however, is that the functional form representing the radiance profile must be smooth. Evidently, the sixth-degree polynomial shows fluctuation between points, while the fifth-degree polynomial is much smoother. In view of the preceding, the optimal degree of the polynomial is determined based on the smoothness of the polynomial and the accuracy of the fitting. A fifth-degree polynomial is found to be the best functional form for the application of DI to temperature retrievals.

d. *Adjustment of radiances*

Previous studies show that applications of the DI using simulated HIRS radiances without adjustments produce large errors ($\sim$5 K; Ou and Liou 1989). These errors occur because the problem of remote sounding of temperature is nonlinear. In addition to the cloud effect, the main sources of nonlinearity are the dependence of the transmittance on temperature, the dependence of the Planck intensity on wavenumber within the spectrum of a sensing channel, the dependence of the Planck intensity on wavenumber between spectral bands, the dependence of the transmittance on the concentration of absorbing gases and aerosols, and the model constraints.

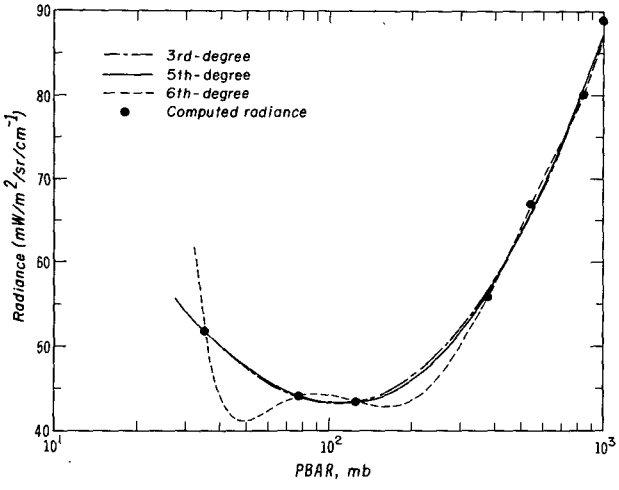

FIG. 7. Fitting of the simulated radiances for HIRS channels 1–7 by third-, fifth-, and sixth-degree polynomials.

Since DI is a linear transform method, these nonlinear factors must be eliminated before performing retrieval. We have described a method to remove cloud contamination in satellite data in the previous section. The remaining nonlinear factors may be removed by adjusting radiances to simulate a nonexistent but mathematically consistent "linear" radiance profile. Ou and Liou (1989) have proposed an adjustment scheme in terms of a "scaling factor," which encompasses the effects of variations in the sharpness index, surface discontinuity of temperature, and channel properties. The present adjustment process is a further improvement of this scheme. We first define the "linear" radiance, which is the computed radiance using the generalized weighting function profile with uniform κ for all channels, and the polynomial fitting of the Planck intensity profile at a reference wavenumber above the surface. Different sets of linear radiances can be derived based on the mean κ values shown in Fig. 6 and can be directly used in the DI for temperature retrieval.

The reason that the range of the polynomial fitting of the Planck intensity profile must be above the surface is discussed below. As shown in section 2, the DI is developed for an infinite atmosphere. The real atmosphere, however, is semi-infinite with the surface as the lower boundary. In section 2, we have demonstrated that the radiative transfer equation [Eq. (1)] may be transformed to an equation simulating an infinite atmosphere [Eq. (4)]. The basic assumption is that the slab below the earth surface may be viewed as a semi-infinite isothermal emitter. In addition, discontinuity always occurs between the surface temperature and the surface air temperature. Polynomial expressions, which are obtained by numerical fitting of the full-range ($p = 0$ to $p \rightarrow \infty$) Planck profile, generally cannot adequately represent this discontinuity and the assumed behavior of constant temperature below the surface. Figure 8 illustrates this point. The solid and dotted lines are the HIRS channel 7 Planck profile and weighting function based on the U.S. standard temperature profile, respectively. The dashed line is the fifth-degree polynomial which covers the full range of the Planck profile for 30 mb $< p <$ 2000 mb. Clearly, this fitting is not entirely satisfactory. The below-surface constant temperature was not reproduced well. Significant temperature deviations also occur in the stratosphere. The fifth-degree polynomial, however, fits the temperatures in the pressure range from 30 to 1000 mb rather well, but the portion of the polynomial for $p >$ 1000 mb deviates from constant behavior. This deviation can be accounted for by the adjustment of

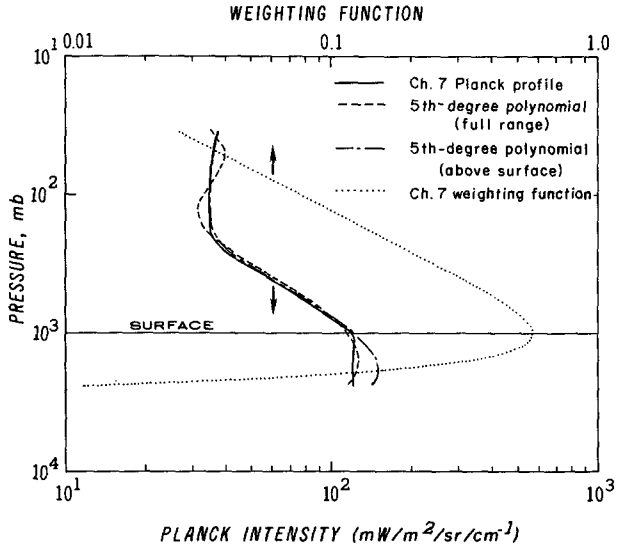

FIG. 8. Fittings of the HIRS channel 7 Planck intensity profile base on the U.S. standard temperature profile. The channel 7 weighting function is also shown.

radiances. Based on the preceding numerical experimentations, the linear radiance is evaluated using the fifth-degree polynomial, which is applicable to the Planck intensity profile above the surface.

To relate the observed (referred to here as "simulated") radiances to linear radiances, we use the BUAN temperature profiles and the transmittance model to perform simulations. We select 700 cm^{-1} as a reference wavenumber and use the mean κ value of channel 7 determined in section 5b. The 700-cm^{-1} Planck intensity profile based on the atmospheric ($p < p_s$) temperature field is fitted to a fifth-degree polynomial. Then from Eq. (17), the coefficients of the polynomial, a_m, are determined. Finally, linear radiances are computed from Eq. (16).

The simulated radiances are computed from Eq. (1) using the weighting functions that are evaluated from the transmittance model. We found that the correlation between simulated and linear radiances for each channel is significant, with the exception of channel 16. This exception may be due to the fact that the weighting function of channel 16 peaks near the tropopause at about 200 mb where the temperature inversion occurs (Fig. 6). In the present retrieval, the data involving channel 16 is not used. The radiance correlations for channels 6, 7, and 13 are particularly significant, presumably due to the narrow form of the weighting function of these channels.

Linear radiances can be related to simulated radiances in quadrature form:

$$R_{il} = a_i + b_i R_{is} + c_i R_{is}^2, \qquad (26)$$

where R_{il} and R_{is} denote linear and simulated radiances, respectively. Table 1 lists the values of a_i, b_i, and c_i along with the rms differences between the model-computed and fitted values of R_{il}. The rms differences between linear and simulated radiances are less than 1.0 and 1.3 mW m^{-2} sr^{-1} cm^{-1}, for the 15- and 4.3-μm channels, respectively. The percentage errors corresponding to these rms errors are less than 2%. This indicates that the linear and simulated radiances are highly correlated. The coefficients a_i, b_i, and c_i are set before the performance of retrieval. As pointed out previously, the conversion of simulated (or observed) radiances to linear radiances is to eliminate nonlinear factors contained in simulated radiances, so that the DI can be used for realistic temperature retrieval.

6. Retrieval results and discussions

Using the BUAN collocated satellite and radiosonde data, we have performed temperature retrievals using the DI. We have selected two groups of data for this study. Group 1 consists of 1000 profiles that were collected between 3 April and 7 April 1988. The sounding profiles are used to establish parameterizations in the cloud-removal method (section 4), and in the adjustment of radiances (section 5). Group 2 consists of another 1000 profiles that were collected between 7 April and 12 April 1988. The satellite data of both groups are used to test the DI for clear retrievals and for the cloud-removal scheme developed in this paper. These tests use parameterizations developed from group 1 data.

Based on the N^* values given in the BUAN data, the profiles have been separated into three categories: clear ($N^* = 0$), partly cloudy ($0 < N^* < 1$), and overcast ($N^* > 1$). Table 2 lists the geographical distribution of the three categories of profiles in group 1. We have divided the globe into five geographic zones. More than 50% of the cases are clear. About 20% of the cases are identified as partly cloudy. A major portion of the data (~33%) is in the northern midlatitude area (60°–30°N), where the density of the radiosonde stations is the highest among the five geographic zones.

TABLE 1. Coefficients in the correlation between the simulated and linear radiances and rms differences between computed and linear radiances.

Channel	a	b	c	rms difference (mW m^{-2} sr^{-1} cm^{-1})
1	101.22	−3.16	0.0407	0.62
2	−16.66	1.35	−0.0016	0.37
3	−70.85	3.46	0.0214	0.60
4	−9.19	1.68	−0.0110	0.91
5	10.96	0.75	0.0004	0.74
6	−2.53	1.21	−0.0016	0.28
7	−3.51	1.37	−0.0024	0.77
13	51.30	51.63	−12.02	1.29
14	46.65	51.26	−14.92	1.26
15	42.41	45.68	−33.45	1.22
17	31.26	303.30	−827.9	0.80

TABLE 2. Geographic distribution of selected data.

Geographic zone	Number of profiles			
	Clear	Partly cloudy	Overcast	Total
90°–60°N	168	36	36	240
60°–30°N	130	91	101	322
30°N–30°S	173	47	56	276
30°–60°S	66	10	36	112
60°–90°S	23	13	14	50
Ocean	472	158	171	801
Land	88	39	72	199
Total	560	197	243	1000

In addition, about 80% of all the data is collected over coastal areas and oceans.

Temperatures are retrieved at the peak pressure level of each channel (Fig. 6). These peak pressure levels are located at 11 layers between 17 and 1000 mb. Temperature differences between the retrieved and sounding values are computed at each peak pressure level as follows:

$$\Delta T_j = T_{\mathrm{DI},j} - T_{sd,j}, \tag{27}$$

where T_{DI} and T_{sd} denote the retrieved and sounding temperatures, respectively, and j denotes the index of peak pressure level. The sounding values have been obtained by interpolation of the BUAN sounding data at the 15 mandatory and 25 significant levels. Sounding values are not available at all levels for all profiles. About 10% of the cases have no sounding values. Thus computation of temperature differences can only be carried out at those levels with available sounding data. Once temperature differences at each pressure level are calculated, two-point averages are carried out to obtain the layer-mean temperature differences:

$$\overline{\Delta T_j} = \frac{\Delta T_j + \Delta T_{j+1}}{2}, \tag{28}$$

where the overbar denotes the layer mean between the jth and the $(j+1)$th levels.

Figure 9 shows a schematic description of the atmospheric temperature retrieval using the DI. Observed clear radiances are converted to linear radiances via a universal equation [Eq. (26)], where nonlinear factors such as variations in κ for HIRS channels are filtered out. Linear radiances are then used to evaluate the coefficients a_m in Eq. (16). Subsequently, the Planck intensities are determined from Eq. (17).

Simulation retrievals are carried out using the linear radiances as input. The purpose of these retrievals is to examine the effects of errors on the polynomial fitting of radiances of the retrieval performance. Linear radiances have been generated according to the definition described in section 5d. It is noted that all nonlinear factors have been largely removed from these linear radiances. Thus retrievals using linear radiances as input are reduced to mathematical problems. Since Eq. (12) is exact, retrieved Planck intensity values should be identical to polynomial values used in generating the linear radiances [Eq. (17)]. However, since polynomial fitting has errors, values of $B(\tilde{\xi})$ deviate from the true Planck intensity profile. These fitting errors are the only possible error sources in the retrieved temperature values.

For each layer and geographical zone, we compute the sample-mean temperature bias:

$$D_{ij} = \frac{1}{N_{ij}} \sum_{n=1}^{N_{ij}} \overline{\Delta T_{ijn}}, \tag{29}$$

where $\overline{\Delta T_{ijn}}$ and N_{ij} are the layer-mean temperature difference and the total number of profiles for the jth layer in the ith geographical zone, respectively. Table 3 shows values of D_{ij}. The linear radiances are generated from group 1 sounding data using the fifth-degree polynomials to fit the Planck intensity profiles. For each geographical zone, the vertical variation of D_{ij} shows an alternating pattern. Near the surface and in the upper troposphere and the lower stratosphere, $D_{ij} > 0$. In the lower troposphere and upper stratosphere, $D_{ij} < 0$. In particular, maximum D_{ij} values (approximately 6 K in polar region, and 5 K in tropical region) occur near the tropopause, because polynomial fittings are unable to resolve the sharp temperature inversions.

To investigate the effects of adjustment errors and instrument noises, we perform retrieval exercises using three sets of input radiances. Linear radiances are generated using the sounding data of the fifth-degree polynomial fittings of Planck intensity profiles. Simulated radiances are generated using the sounding data and Eq. (1). BUAN radiances are obtained by converting clear or cloud-removed brightness-temperature data in the BUAN files to radiances. Note that both simulated and BUAN radiances require the application of adjustment procedures via Eq. (26). Retrieval results are presented in terms of layer-mean rms temperature differences. For linear and simulated retrievals, all cases are included. For retrievals using BUAN radiances, only clear and partly cloudy cases are included. In all cases, D_{ij}'s for each layer and geographical zone listed in Table 3 are subtracted from the retrieved temperature values. Figure 10 shows the vertical distribution of rms temperature differences for the three sets of retrievals. The rms differences for all three sets are close to 2 K between 100 and 700 mb. The larger differences ($\sim$2.2–3 K) for $p < 100$ mb are mainly due to inversions near the tropopause for tropical areas. The rms differences for retrieval using linear radiances are less than 2 K for $p > 100$ mb. These differences are caused by the residual effects of polynomial fluctuation around the sounding profile. The rms differences from simulated retrievals are slightly larger (by less than 0.5 K) than those from linear retrievals. The increase in rms differences is mainly due to uncertainties in the use of

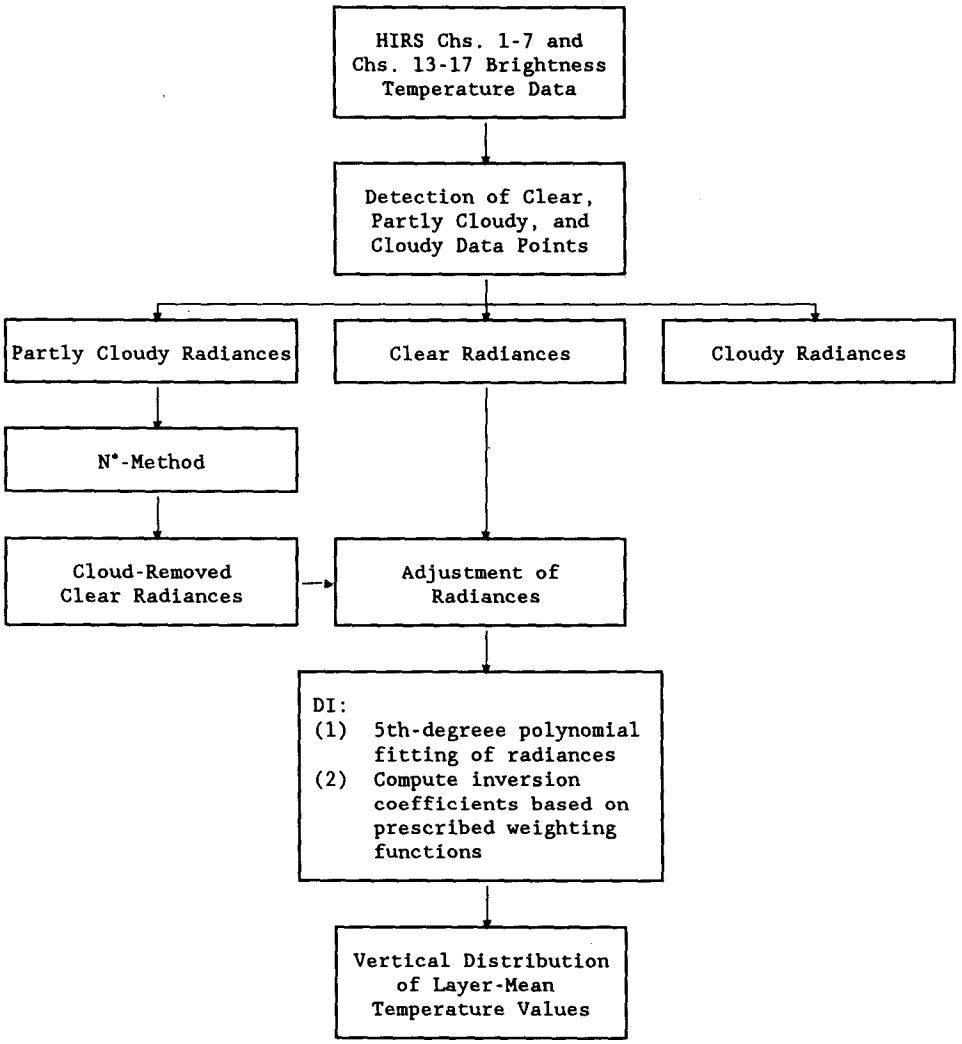

FIG. 9. A schematic description of the atmospheric temperature retrieval using the DI.

Eq. (26). Finally, the rms differences from using BUAN radiances are also slightly larger (by less than 1 K) than those from simulated retrievals. The larger rms differences in the case of BUAN radiances, particularly in the lower troposphere, are results of instrument noise, and errors in the weighting function of the near-surface channels (channels 6, 13, and 7). It appears that between 100 and 700 mb the effects of correlation,

TABLE 3. Values of D_{ij} for each layer and geographical zone where sounding values are available.

Layer index	Pressure range (mb)	D_{ij} (K)							
		90°–60°N	60°–30°N	30°N–30°S	30°–60°S	60°–90°S	Ocean	Land	All
1	28–78	0.6	0.72	−5.45	−1.68	1.28	−0.91	−0.58	−0.85
2	78–93	−1.78	−1.75	−1.98	−1.74	−1.42	−1.72	−2.17	−1.81
3	93–175	−3.26	−3.13	4.23	0.76	−3.55	−0.62	−1.23	−0.74
4	175–325	−1.1	−0.66	4.95	1.39	−2.13	0.80	1.41	0.93
5	325–375	4.13	3.54	2.06	1.74	3.39	2.99	3.30	3.05
6	375–535	6.08	3.90	−0.92	1.55	6.39	3.09	2.49	2.97
7	535–740	1.43	0.21	−1.74	−0.12	1.41	0.09	−0.34	0.01
8	740–815	−3.35	−2.30	−1.22	−1.28	−2.55	−2.21	−1.92	−2.14
9	815–975	−4.14	−2.07	0.13	−0.98	−1.90	−2.09	−0.88	−1.84
10	975–1000	0.07	0.13	0.91	0.27	0.36	0.27	0.65	0.35

instrument noise, and error in the weighting function on resulting rms differences are smaller than the effects produced by polynomial fitting.

The effects of different degrees of polynomial fitting in the adjusted radiances are subsequently investigated. Figure 11 shows the rms differences from linear retrievals using fourth-, fifth-, and sixth-degree polynomials. The sixth-degree polynomial fittings yield the smallest rms differences, while the fourth-degree polynomial fittings yield the largest differences, because the accuracy in fittings of radiances increases with the degree. The rms differences from the sixth-degree fittings are from 0.5 to 1.5 K and are smaller than the fifth-degree fittings by 0.2–1 K for $p > 100$ mb. It appears that the sixth-degree polynomials should yield the best retrieval performance using measured radiances. However, Fig. 12 shows the opposite results. Shown in the plot are the rms differences from retrievals using BUAN radiances. The sixth-degree polynomial fittings yield the worst retrieval performances. The rms differences vary from 2 to 4 K. Apparently, uncertainties in radiances caused by the adjustment procedure deteriorate retrieval performances. In this case, the ill-conditioned characteristics of the retrieval problem become more significant for retrieval using the higher-degree polynomial. On the other hand, rms differences from retrievals using the fifth-degree polynomials are better (by less than 0.5 K) than those from using the fourth-degree polynomials. This is expected since the fourth-degree polynomials fit the radiance profiles less satisfactorily.

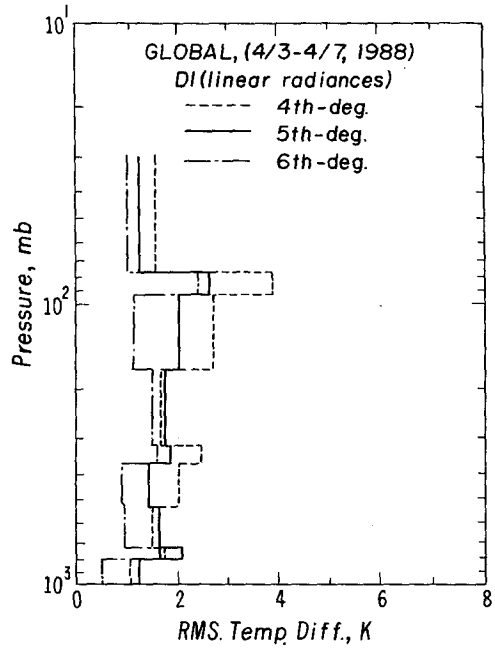

FIG. 11. The vertical distributions of rms differences from temperature retrievals using linear radiances generated using fourth-, fifth-, and sixth-degree polynomials.

To compare the DI with the BUAN MV scheme, Fig. 13 shows the vertical distributions of rms differences for the two schemes using BUAN radiances. Also shown are the rms differences for the BUAN first guess.

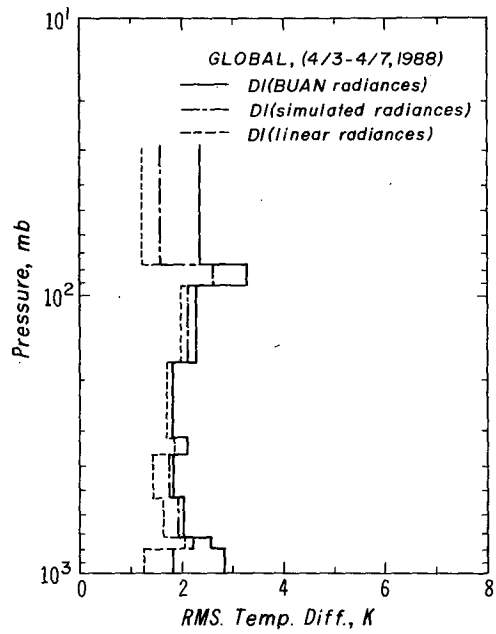

FIG. 10. The vertical distributions of rms differences from temperature retrievals using linear, simulated, and BUAN radiances as input.

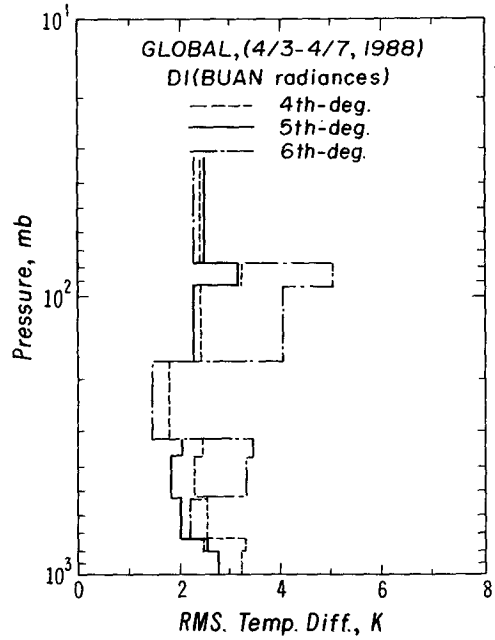

FIG. 12. The vertical distributions of rms differences from temperature retrievals using BUAN radiances generated using fourth-, fifth-, and sixth-degree polynomials.

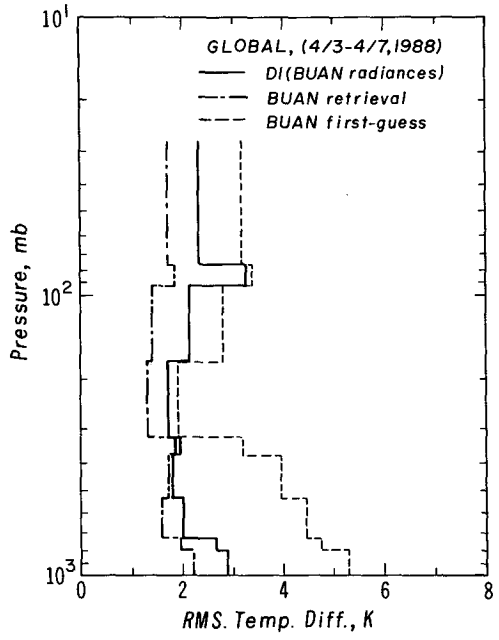

FIG. 13. The vertical distributions of rms temperature differences from the DI and BUAN schemes using the same BUAN radiances.

Except for $p > 800$ mb, the rms differences for the MV are between 1 and 2 K. For $p > 100$ mb, the rms differences for the DI are larger than the differences for the MV scheme by less than 1 K. For $p > 500$ mb, the larger rms differences for the DI are probably caused by the adjustment procedure. For 300 mb $< p < 500$ mb, accuracies of the DI and of the MV are about the same. For $p < 300$ mb, the larger rms differences for DI are produced by polynomial errors near the tropopause. The aforementioned results indicate that the DI is generally comparable to the MV. The DI requires neither a first-guess profile nor the error covariance matrices to regulate solutions. The rms differences for the BUAN first guesses, as shown in Fig. 13, range between 2 K in the upper troposphere and 5 K near the surface. The rms differences for DI are less everywhere than those for the BUAN first guesses. Thus, it appears that DI can also be used as an efficient scheme to obtain the first-guess profiles for the MV. No cumbersome library search procedures are required.

To investigate the effects of applying the adjustment parameterizations (Table 1) and the temperature biases (Table 3) to different satellite datasets, we compare retrieval results from group 1 (3 April–7 April 1988) and group 2 (7 April–12 April 1988). Figure 14 shows the rms differences from the two sets of retrievals. It is noted that rms differences from these two sets differ by no more than 0.2 K. This slight difference implies that the adjustment parameterizations and mean biases are applicable to different sets of satellite data which are collected in a period of less than 10 days. The values of the mean temperature biases may vary over a longer period. However, the adjustment parameterizations should be applicable for a long time period, because they depend more on channel characteristics than on temperature and humidity profiles.

To test the multispectral cloud-removal scheme described in section 4, we have also carried out retrievals using the DI under partly cloudy conditions. Figure 15 shows the vertical distributions of rms differences for partly cloudy retrievals using the DI and the MV. Two sets of radiances are employed as inputs in the DI. One set is the BUAN radiances that were obtained by the BUAN cloud-removal method. The other set is the cloud-removed clear radiances from the multispectral method. The rms differences for BUAN first-guess profiles are also shown. To ensure the assumption that the same cloud properties over the adjacent pixels are valid, only about 50 partly cloudy cases were selected for retrieval. These cases involve differences in channel 7 radiances over adjacent points larger than about 20 mW m^{-2} sr^{-1} cm^{-1}. McMillin (1978) also noted that the clear radiances determined for cases with larger differences in the window channel radiance are expected to be closer to true values. Similar to Fig. 13, the rms differences for BUAN MV retrievals are between 1 and 2 K for $p < 800$ mb. The rms differences from the DI using BUAN radiances are close to those from the MV, between 200 and 700 mb. The larger rms differences near 90 mb are due to uncertainty in the retrieved tropopause temperature over tropical areas. By comparing rms differences from the DI using two sets of radiances, we see that the present multispectral method produces larger rms differences than

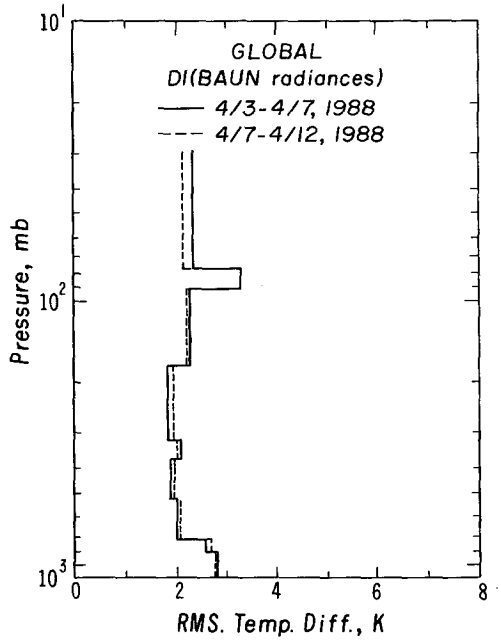

FIG. 14. The vertical distributions of rms temperature differences from temperature retrievals using two different datasets.

the BUAN N^* method (~0.5 K). Between 100 and 700 mb, the rms differences for the DI using the multispectral method are about 2.5 K.

The operational N^* method uses the combined 4.3-μm and microwave channels to determine N^* over the oceans. Over land, only 4.3-μm channels can be used. As a comparison, Table 4 lists the vertically averaged rms differences for both the DI and MV over land. It is well known that temperature retrievals over land are less satisfactory due to the nonhomogeneity of surface temperature. The table shows that the vertically averaged rms differences are all larger than 2 K. Using the same BUAN radiances, the average rms difference for the DI is larger than that for the MV by 0.37 K. Using the MV with two different cloud-removal schemes in the retrieval, the vertically averaged rms difference is only 0.09 K. The performance of the present multispectral cloud-removal scheme is comparable to the BUAN N^* method over land.

TABLE 4. Vertically averaged rms temperature differences for both DI and MV partly cloudly retrievals over land.

MV		DI	
First guess	Retrieved	BUAN radiance	Channels 6–8 radiance
4.95 K	2.40 K	2.77 K	2.86 K

7. Summary and conclusions

We have tested the applicability of the DI to temperature retrievals using measured satellite data. We first reviewed the fundamentals of the DI and formulated the radiative transfer equation that is appropriate for an infinite atmosphere. The convolution theory of bilateral Laplace transform was subsequently used to derive an expression for the local Planck intensity value. The Planck intensity in real space can be exactly expressed as a linear sum of the higher-order derivatives of radiance profiles. The inversion coefficient in each term of the summation can be obtained based on a generalized form of weighting functions. The higher-order derivatives of radiance profiles can be obtained by fitting the radiances for a finite number of channels using a polynomial function.

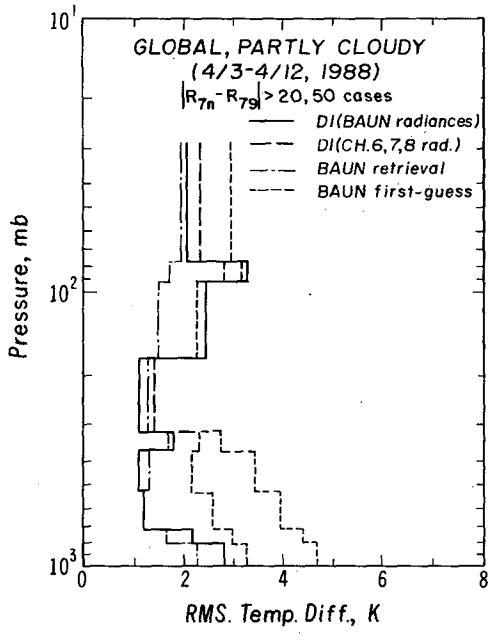

FIG. 15. The vertical distributions of rms temperature differences for partly cloudy conditions using the DI and BUAN schemes. Two sets of radiances are used in DI; one is the cloud-removed radiances by the current multispectral cloud-removal method, while the other is the cloud-removed radiances by the BUAN N^* method.

The satellite dataset used in the present study contains collocated brightness-temperature and radiosonde data that have been collected during the period of the BUAN experiment. The brightness-temperature data include both cloud-contaminated and clear cases. Cloud-removed clear brightness temperatures obtained from the operational N^* method are also included. The satellite dataset also contains the first-guess and retrieved temperature profiles.

A new cloud-removal method has been developed in conjunction with the DI. This method reconstructs clear radiances from cloud-contaminated brightness temperatures using the principle of the N^* method. The present method uses the radiances of HIRS channels 6, 7, and 8 to determine clear radiances and surface temperature simultaneously, based on radiative transfer simulations. In this multispectral method, radiance relationships for the three channels are first developed. The linear relationships between partly cloudy radiances for the two sets of channels are subsequently used to derive a separate set of clear-radiance equations. The parameterized equations are solved simultaneously using an iterative approach.

We have selected HIRS channels 1–7 and 13–17 to carry out temperature retrievals using the DI. The large radiosonde dataset along with a transmittance model are employed to compute a set of weighting function profiles. Each profile is then fitted to the generalized form to obtain the sharpness index parameters and peak pressure levels. The average values of these parameters are used in the retrievals. The strategy in determining the optimal degree of polynomial to be used in retrievals is subsequently discussed. To apply the DI, which is a linear inversion method, to a nonlinear temperature retrieval problem, we have developed an adjustment scheme to derive linear radiances from satellite data. We compute a large number of linear and simulated radiances based on forward radiative transfer calculations. For each channel, a parameterization in the form of quadrature fitting is established between the linear and simulated radiances. These parameter-

izations are used to convert measured (or simulated) radiances to linear radiances, thus removing major nonlinear components from the data. The rms differences between the computed and fitted linear radiances are generally less than 1.3 mW m^{-2} sr^{-1} cm^{-1}, indicating that the linear and simulated radiances are highly correlated.

Comparisons of the retrieval results using linear, simulated, and BUAN radiances illustrate the effects of radiance adjustment, instrument noise, collocation error, and model error. The retrieval results from the DI are comparable to those from the MV. We also demonstrate that the multispectral cloud-removal method can be particularly useful for the determination of surface temperature over land, where the application of microwave techniques may be questionable. Because the DI does not require first-guess profiles, it may be used to retrieve large amounts of temperature profiles efficiently.

Acknowledgments. This research was supported by the Geophysics Directorate, Air Force Systems Command, under Contract F19628-90-K-0004. We are grateful to Dr. L. M. McMillin and Mr. Tony Reale of NOAA/NESDIS for providing the collocated BUAN dataset.

REFERENCES

Abramowitz, M., and I. A. Stegun, 1972: *Handbook of Mathematical Functions.* Dover Publications, Inc., 1046 pp.

Bloom, H. J., and A. J. Nappi, 1990: The effect of a reduced sample of time and space coincident satellite/radiosonde collocations on retrieval accuracy statistics. Preprints, *Fifth Conference on Satellite Meteorology and Oceanography,* Amer. Meteor. Soc., London, 64–68.

Burroughs, W. J., 1991: *Watching the World's Weather.* Cambridge University Press, 196 pp.

Chahine, M., 1970: Inverse problems in radiative transfer: Determination of atmospheric parameters. *J. Atmos. Sci.,* **27,** 960–967.

Chandrasekhar, S., 1960: *Radiative Transfer.* Dover Publications, 393 pp.

Chedin, A., N. A. Scott, C. Wahiche, and P. Moulinier, 1985: The improved initialization inversion method: A high resolution physical method for temperature retrievals of the TIROS-N series. *J. Climate Appl. Meteor.,* **24,** 124–143.

Eyre, J. R., 1989: Inversion of cloudy satellite sounding radiances by nonlinear optimal estimation. I: Theory and simulation for TOVS. *Quart. J. Roy. Meteor. Soc.,* **115,** 1001–1026.

Fleming, H. E., M. D. Goldberg, and D. S. Crosby, 1986: Minimum variance simultaneous retrieval of temperature and water vapor from satellite radiance measurements. Preprints, *Second Conf. on Satellite Meteorology/Remote Sensing and Applications,* Williamsburg, VA, Amer. Meteor. Soc., 20–23.

Houghton, J. T., F. W. Taylor, and C. D. Rodgers, 1984: *Remote Sounding of Atmospheres.* Cambridge University Press, 343 pp.

Kalnay, E., M. Kanamitsu, and W. E. Baker, 1990: Global numerical weather prediction at the National Meteorological Center. *Bull. Amer. Meteor. Soc.,* **71,** 1410–1428.

King, J. I. F., 1985: Theory and application of differential inversion to remote temperature sensing. *Advances in Remote Sensing Retrieval Method.* H. E. Fleming and M. T. Chahine, Eds., Deepak Publishing Co., 437–444.

——, and S. J. Leon, 1990: Smooth temperature profile inferencing from noisy radiance data using optical measure theory. Preprints, *Fifth Conf. on Satellite Meteorology and Oceanography,* Amer. Meteor. Soc., London, 78–81.

——, R. G. Hohlfeld, and J. C. Kilian, 1989: Applications and evaluation of a differential inversion technique for remote temperature sensing. *Meteorol. Atm. Phys.,* **41,** 115–126.

McCleese, D. J., and L. S. Wilson, 1976: Cloud top heights from temperature sounding instruments. *Quart. J. Roy. Meteor. Soc.,* **102,** 781–790.

McMillin, L. M., 1978: An improved technique for obtaining clear radiances from cloud-contaminated radiances. *Mon. Wea. Rev.,* **106,** 1590–1597.

——, 1991: Evaluation of a classification method for retrieving atmospheric temperatures from satellite measurements. *J. Appl. Meteor.,* **30,** 432–446.

——, H. E. Fleming, and M. L. Hill, 1979: Atmospheric transmittance of an absorbing gas. III: A computationally fast and accurate transmittance model for absorbing gases with variable mixing ratios. *Appl. Optics,* **18,** 1600–1606.

Menzel, W. P., W. L. Smith, and T. R. Stewart, 1983: Improved cloud motion wind vector and altitude assignment using VAS. *J. Appl. Meteor.,* **22,** 377–384.

Ou, S. C., and K. N. Liou, 1989: Remote sounding of atmospheric temperature profiles using the optical measure method. Report, AFGL-TR-89-0346, Air Force Geophysics Laboratory, 64 pp.

——, ——, and J. I. F. King, 1990: Remote sounding of temperatures in cloudy atmospheres using the differential inversion method. Preprints, *Fifth Conf. on Satellite Meteorology and Oceanography,* Amer. Meteor. Soc., London, 60–63.

Pearson, C. E., 1974: *Handbook of Applied Mathematics.* Van Nostrand Reinhold Co., 87–89.

Phillips, N., J. Susskind, and L. M. McMillin, 1988: Results of a joint NOAA/NASA sounder simulation study. *J. Atmos. Oceanic. Technol.,* **5,** 44–56.

Reale, A. L., H. E. Fleming, D. Q. Wark, C. S. Novak, F. S. Zbar, J. R. Neilon, M. E. Gelman, and H. J. Bloom, 1990: Baseline Upper Atmospheric Network (BUAN) evaluation: Final report. *NOAA Tech. Rep., NESDIS,* **52,** 57 pp.

Smith, W. L., 1968: An improved method for calculating tropospheric temperature and moisture from satellite radiometer measurements. *Mon. Wea. Rev.,* **96,** 387–396.

——, 1970: Iterative solution of the radiation transfer equation for the temperature and absorbing gas profile of an atmosphere. *Appl. Opt.,* **9,** 1993–1999.

——, and C. M. R. Platt, 1978: Comparison of satellite-deduced cloud heights with indications from radiosonde and ground-based laser measurements. *J. Appl. Meteor.,* **17,** 1796–1802.

——, H. M. Woolf, C. M. Hayden, D. Q. Wark, and L. M. McMillin, 1979: The TIROS-N Operational Vertical Sounder. *Bull. Amer. Meteor. Soc.,* **60,** 1177–1187.

——, H. L. Huang, S. A. Ackerman, and H. E. Revercomb, 1990: Sounding through semi transparent cloud with high resolution infrared radiance spectra. Preprints, *Fifth Conf. on Satellite Meteorology and Oceanography,* Amer. Meteor. Soc., London, 55–59.

Widder, D. V., 1971: *An Introduction to Transform Theory.* Academic Press, 253 pp.

Wielicki, B. A., and J. A. Coakley, 1981: Cloud retrieval using infrared sounder data: Error analysis. *J. Appl. Meteor.,* **20,** 157–169.